Microsyst Technol (2015) 21:739–747
DOI 10.1007/s00542-014-2234-4

TECHNICAL PAPER

Realization of a micro pressure sensor with high sensitivity and overload by introducing beams and Islands

Zhongliang Yu · Yulong Zhao · Lili Li · Cun Li · Yan Liu · Bian Tian

Received: 2 January 2014 / Accepted: 28 May 2014 / Published online: 19 June 2014
© Springer-Verlag Berlin Heidelberg 2014

Abstract Presented is a piezoresistive absolute micro pressure sensor for altimetry. This investigation involves the design, fabrication and testing of the sensor. By analyzing the stress distribution of sensitive elements using finite element method (FEM), an improved structure is built up through introducing multi islands and sensitive beams into traditional flat diaphragm. The proposed configuration presents its advantages in terms of enhanced sensitivity and overload resistance compared with the bossed diaphragm and flat diaphragm structures. Multivariate fittings based on ANSYS® simulation results are performed to establish equations about surface stress and deflection of the sensor. Optimization by MATLAB® is carried out to determine the structure dimensions. Silicon bulk micromachining technology is utilized to fabricate the sensor prototype, and the fabrication process is discussed. The output signals under both static and dynamic conditions are evaluated and tested. Experimental results demonstrate the sensor features a relatively high sensitivity of 17.795 μV/V/Pa in the operating range of 500 Pa at room temperature and a proper overload resistance of 200 times overpressure to promise its survival under atmosphere. The favorable performances enable the sensor's application in measuring absolute micro pressure.

1 Introduction

The micro-fabricated piezoresistive pressure sensor is one of the best developed MEMS devices in use today (Eaton and Smith 1997). It has been widely applied due to the excellent linearity, fine sensitivity, simple and direct signal transduction mechanism (Barlian et al. 2009; Sze 1994; Chang 2008). As the technology of aerospace engineering advances, a number of piezoresistive pressure sensors are desired for micro pressure measurements (Ko et al. 2007; Reynolds et al. 2000; Mackowiak et al. 2010; Tian et al. 2012; Berns et al. 2006). Based on the relationship between pressure and height, the aircraft altimetry can be obtained through measuring pressure. Because of the extremely low pressure in high altitude, high sensitivity is needed to ensure the accuracy of orbital correction. Besides, a high overload resistance is required for a micro-pressure sensor to suffer atmosphere on the earth. To develop a micro pressure sensor with high sensitivity and overload resistance is of importance and necessity for aerospace. To some degree the chip structure determines the sensitivity, linearity, and overload resistance (Guiming et al. 2011; Mackowiak et al. 2010; Tian et al. 2012). The lower the pressure range is, the thinner the diaphragm is needed to maintain high sensitivity. However, excessively thin membrane may induce large deflection and instability, leading to unfavorable performances of a sensor such as linearity, safety factor, and etcetera (Lin et al. 1999). Therefore, the structure design of a sensor chip is critical.

Improvements in sensing configuration design have made the performances of sensors better. Shimazoe et al. (1982) developed a sensor with a center boss on the diaphragm and an annular groove formed on the back surface. The accuracy was 0.17 % FS, while the variation of stress distribution was evident, thus the high precision placement of piezoresistors was demanded. Moreover, the sensor was unfavorable to miniaturization and batch production. Bao et al. (1990) proposed a beam-diaphragm structure by introducing beams on the flat membrane of twin isles

Z. Yu · Y. Zhao (✉) · L. Li · C. Li · Y. Liu · B. Tian
State Key Laboratory for Manufacturing Systems Engineering, Xi'an Jiaotong University, Xi'an 710049, Shaanxi, People's Republic of China
e-mail: zhaoyulong@mail.xjtu.edu.cn

structure, forming a shape like dumbbell. The nonlinearity of 0.25 % FS was relatively low, but the sensitivity of 0.6901 μV/V/Pa was slightly lower for the operating range of 1 kPa, and the overload resistance was lower due to the lack of thick islands in the rear cavity. Johnson et al. (1992) reported a novel ribbed and bossed structure. The incorporation of rib into the diaphragm for stress concentration was proved to be effective in enhancing sensitivity and reducing deflection. Additionally, the introduction of a self-aligning rim was favorable to the enhancement of manufacture. However, the overload resistance was a bit lower due to the thin bosses. Tian et al. (2012) designed a beam-membrane structure through etching the cross beam on the diaphragm resulting in a good linearity (the nonlinearity was 0.09 % FS) for the measurements of 5 kPa, while the overload resistance and the sensitivity of 1.549 μV/V/Pa were relatively low.

To measure the absolute micro pressure, both high sensitivity and high overload resistance are required. Moreover, a simple fabrication process is needed for high yield and low cost. As the existing design schemes discussed above fail to fully meet the requirements, a beam-membrane-quad-island (BMQI) structure is put forward. By incorporating beams into the diaphragm, stresses are expected to be concentrated. High overload resistance is also anticipated due to the introduction of islands to limit displacement. In addition, silicon bulk micromachining is to be utilized for high yield and low cost. To verify the scheme, FEM model, structure optimization and experiments are implemented.

2 Sensor design

2.1 Structure design

Since absolute micro pressure sensors have to bear atmosphere on the earth, which is hundreds of times higher than operating range, the silicon structure can be easily fractured under such a high overload. In view of the situation, the conventional bossed diaphragm should be taken into account. Due to the mass bulks' support, the membrane may stand atmosphere without breaking. However, the enhancement of overload resistance partly sacrifices the effective stress that reflects sensitivity. To satisfy both of the demands for high sensitivity and overload resistance, a BMQI structure is raised as shown in Fig. 1. The structure is intended for measuring pressure lower than 500 Pa.

2.2 Structure parameters optimization

In order to optimize and determine the structure dimensions, formulas should be deduced. Owing to the existence of beams on the membrane, theoretical formulas are difficult to derive, while the approximate ones can be drawn by the combination of FEM calculation and multivariate fitting.

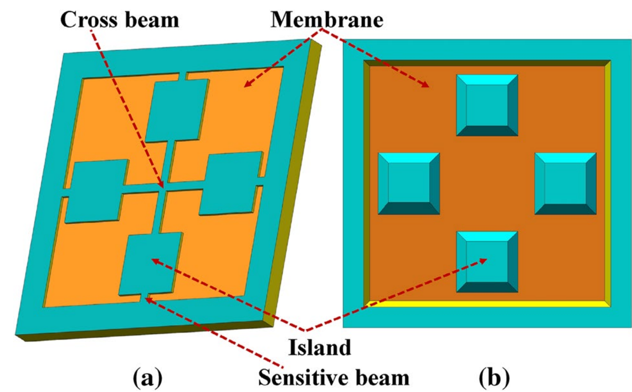

Fig. 1 **a** The schematic diagram of the front view of the BMQI structure. **b** The rearview of the structure without bonding glass

For convenience of illustration, the front view and the cross-sectional view along A–A marked with dimension variables are displayed in Fig. 2, where L refers to the effective width of membrane; D the distance of two opposite islands; I the top width of islands, I_b the bottom width of islands; W the beams' width; t the length of sensitive beams. Additionally, H and B represent the thickness of membrane and beams respectively. In this figure, one of the piezoresistors arranged on a sensitive beam is enlarged. Besides, the glass base on the backside can be observed in the cross-sectional view.

The mechanical stress and the maximum deflection of conventional flat diaphragm (C-type) structure are the power functions of each variable (Young 1986).

Therefore, the differential stress of BMQI is assumed as:

$$\sigma_{\mathrm{d}} = \mathrm{K} \cdot B^{\mathrm{a}} \cdot H^{\mathrm{m}} \cdot I^{\mathrm{n}} \cdot L^{\mathrm{r}} \cdot W^{\mathrm{s}} \cdot t^{\mathrm{q}} \tag{1}$$

where σ_{d} is the difference of x and y direction stress at the center of a resistor, as shown in Fig. 2, when a 500 Pa pressure is applied. B, H, I, L, W, t are the independent dimension variables chosen from the variables described above; K, a, m, n, r, s, q the undetermined constants. To ascertain the constants, the variation of σ_{d} with variables should be studied by ANSYS® loop computation using the standard (100) silicon wafer material properties described in the report by Hopcroft et al. (2010). In the calculation, three values for each variable are assigned in the range listed later. Therefore, 729 loops are needed to cover the entire variable space. Based on the results, multivariate fitting by MATLAB® is carried out. For the simplification, nonlinear fitting is transformed to linear via taking the logarithm of Eq. (1):

$$\ln(\sigma_{\mathrm{d}}) = \ln(\mathrm{K}) + \mathrm{a} \cdot \ln(B) + \mathrm{m} \cdot \ln(H) + \mathrm{n} \cdot \ln(I) + \mathrm{r} \cdot \ln(L) + \mathrm{s} \cdot \ln(W) + \mathrm{q} \cdot \ln(t) \tag{2}$$

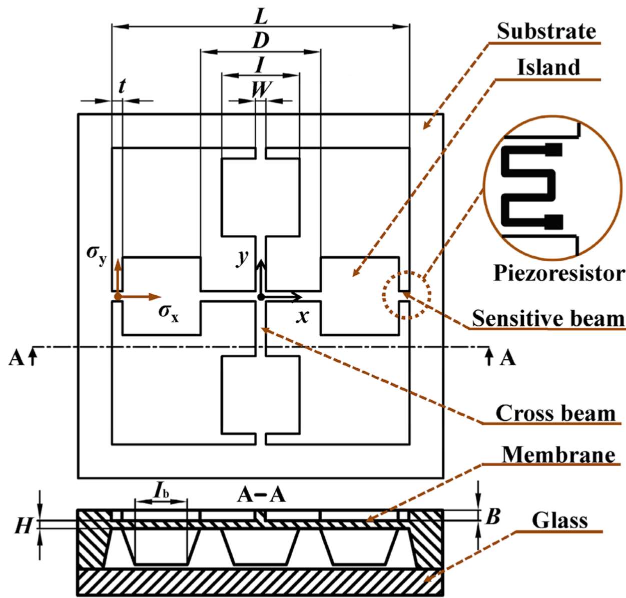

Fig. 2 The front and the cross-sectional views of the BMQI structure

The parameters after logarithm can be regarded as new variables. Hence, a multiple linear regression problem that costs much less is raised and easily solved. To get the constant K in Eq. (1), a nature exponential of the constant item ln(K) in Eq. (2) should be taken. The fitted equation concerning the differential stress σ_d is obtained:

$$\sigma_d = 42.85568\frac{L^{3.24387}}{B^{0.72821}H^{1.24559}I^{0.14835}W^{0.69285}t^{0.17902}} \quad (3)$$

Since the values of deflection have been calculated by ANSYS® in same cycles, the equation about deflection is established based on MATLAB® fitting as stated above:

$$\omega_{\max} = 4.65594 \times 10^{-11}\frac{L^{4.39870}}{B^{1.33615}H^{1.54480}I^{0.14935}W^{0.54189}t^{0.38890}} \quad (4)$$

where $\omega_{\max}$ is the maximum deflection at the center of membrane under the pressure of 500 Pa. In the same manner, namely by the combination of ANSYS® calculation and MATLAB® fitting, the equation related to the condition under overload is established:

$$\sigma_{\text{overload}} = 1.85745 \times 10^6\frac{B^{0.26293}H^{0.19110}I^{0.06102}L^{0.01517}}{W^{0.14454}t^{1.28317}} \quad (5)$$

where σ_{overload} is the maximum von Mises stress under an atmospheric pressure of 100 kPa.To validate the rationality of the hypothesis regarding the functional forms proposed in Eqs. (3), (4) and (5), their coefficients of determination R^2 are calculated to verify the goodness of fit. The values are 0.96686, 0.97821, 0.98751 corresponding to Eqs. (3), (4) and (5) respectively, that demonstrates the fittings are well, thus the ANSYS® calculated results can be almost represented by these three equations. Specifications about the equations discussed are that the ranges of all the variables are constrained by actual demands. Besides, the international system of units is adopted throughout.To optimize the dimensions of BMQI structure, the optimization model is built up:

$$\left.\begin{array}{l} \max(\sigma_d) \\ \text{subject to} \\ \quad \omega\max \le \frac{1}{5}H \\ \quad \sigma_{\text{overload}} \le \frac{\sigma_b}{n} \\ \quad 25\,\mu\text{m} \le B \le 50\,\mu\text{m} \\ \quad 20\,\mu\text{m} \le H \le 30\,\mu\text{m} \\ \quad 1{,}000\,\mu\text{m} \le I \le 1{,}600\,\mu\text{m} \\ \quad 5{,}000\,\mu\text{m} \le L \le 5{,}700\,\mu\text{m} \\ \quad 150\,\mu\text{m} \le W \le 600\,\mu\text{m} \\ \quad 150\,\mu\text{m} \le t \le 350\,\mu\text{m} \\ \quad \sigma_b = 7\,\text{GPa} \\ \quad n = 3.5 \end{array}\right\} \quad (6)$$

where σ_d, $\omega_{\max}$, σ_{overload} have been derived in the Eqs. (3)–(5). σ_b is the ultimate strength of single crystal silicon, n the safety factor, and the ranges of variables B, H, I, L, W, t are listed. According to the small deflection theory, the nonlinearity below 1 % FS can be achieved if the maximum deflection of the flat diaphragm (C-type) structure is kept under one-fifth of the film thickness (Timoshenko and Woinosky-Krieger 1987). For rough reference, the same evaluation of maximum deflection as a constraint of the model is adopted. Through taking the natural logarithms of objective function and constraints in Eq. (6), an equivalent linear optimization problem that apparently simplifies computation is raised. MATLAB® is utilized to search for the optimal solution, and the value of dimension variables are got via taking nature exponentials of the optimization results. By fine adjustment, the sizes of BMQI structure are determined. The sensor die features overall dimensions of 7,000 × 7,000 μm^2, composed of a 20 µm thickness membrane, four 1,500 µm width islands, four 200 µm length, 200 µm width and 30 µm thickness sensitive beams as well as a cross beam with the same width and thickness as sensitive beams.

2.3 Sensor performance evaluation

To evaluate the performance of BMQI sensor with the determined dimensions, ANSYS® is used. The simulation results about the distribution of von Mises stress on sensitive beams and the stress path along the x-axis from the center to the edge of a sensitive beam, when the structure is imposed

500 Pa pressure, are shown in Fig. 3. In the figure, the highest level of stress concentration can be found at the edges of sensitive beams. Therefore, the piezoresistors should be placed near the edges of sensitive beams to obtain high sensitivity.

For comparison of the BMQI structure with the flat diaphragm (C-type) and the bossed diaphragm (E-type) ones, the simulation curves concerning the relationships between differential stress σ_d and applied pressure are plotted in Fig. 4. Through observation of curve slopes, the BMQI obviously presents the highest sensitivity under the dimensions defined in the figure. Furthermore, due to the introduction of beams, the stiffness is increased while the deflection decreased. Thus better linearity can be achieved.

In order to theoretically estimate the concrete value of sensitivity, equation is used to calculate the output voltage (take the resistor oriented in <110> direction on a (100) n-type silicon wafer for example) (Quan et al. 2005; Clark and Wise 1979):

$$U_o(p) \approx \frac{1}{2}\pi_{44}(\sigma_x - \sigma_y)U_i \tag{7}$$

where $U_o(p)$ is the output voltage under pressure p, U_i the input voltage, π_{44} the shearing piezoresistance coefficient. σ_x, σ_y are the longitudinal and transversal surface stress at the central point of resistors as labeled in Fig. 2. Since the concentration of ion implantation is set as 3×10^{14} cm^{-3} less than 1×10^{17} cm^{-3}, π_{44} can be derived as 138×10^{-7} cm^2/N (Tufte and Stelzer 1963). In addition, a series of σ_x and σ_y have been calculated by ANSYS® with the changes of applied pressure p. Therefore, the relationship between applied pressure p and output voltage U_o (p) is derived from Eq. (7):

$$U_o(p) = 6.42362 \times 10^{-5}p \tag{8}$$

where the sensitivity of 32.118 mV/(3 V·500 Pa) is deduced.To assess the influence of vibration on pressure measurements, both modal analysis and dynamic analysis are carried out. FEM simulation shows a bandwidth of 8.398 kHz. Besides, the equation for describing the dynamic performance is derived based on simulation results:

$$U_o(a_z) = 1.63981 \times 10^{-5}a_z \tag{9}$$

where a_z is the acceleration along the z-axis as Fig. 10 shows, U_o (a_z) the output voltage under a_z applied. In the simulation, a maximum acceleration a_z of 15 g is exerted due to the human extreme limit.

3 Fabrication

The BMQI sensor is fabricated based on the bulk micromachining, from a standard double side polished n-type (100) silicon wafer, whose resistivity is around 6,000–8,000 Ω·cm and thickness is 400 μm.

The specific fabrication process flow is illustrated in Fig. 5. Firstly, photolithography is employed to pattern piezoresistors on the front side of the silicon wafer, after SiO_2 layers are grown on both sides of the substrate by thermal oxidation. Then, ion implantation of boron is carried out with a concentration of 3×10^{14} cm^{-3}, forming a sheet resistance of 220 Ω, followed by heavy born ion diffusion. Subsequently, the passivation layers of Si_3N_4, SiO_2 are deposited successively by means of low pressure chemical vapor deposition (LPCVD) and plasma enhanced chemical vapor deposition (PECVD). Contacts are then photo patterned and etched on the front side utilizing reactive ion etching (RIE). In order to activate the boron ion electrically and make dopant uniform, the annealing technology is executed at 1,100 °C for 30 min under nitrogen atmosphere.

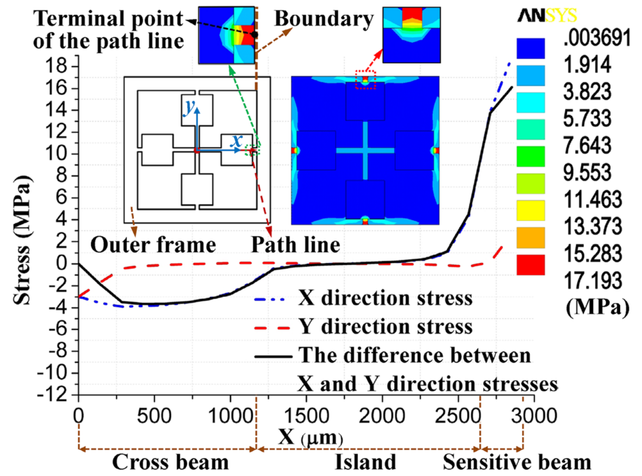

Fig. 3 Simulation about stress distribution and stress path of BMQI

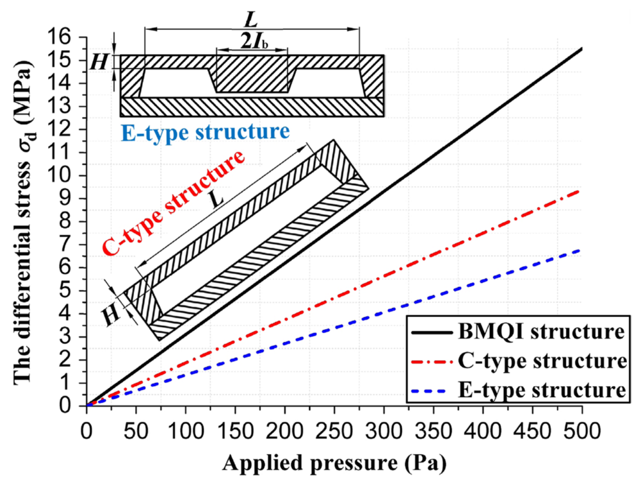

Fig. 4 Comparison of three type structures' differential stresses

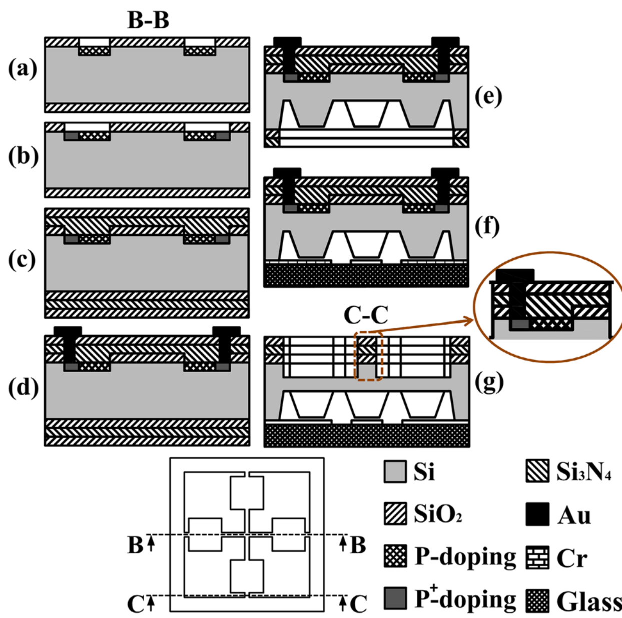

Fig. 5 The schematic of the main process flow

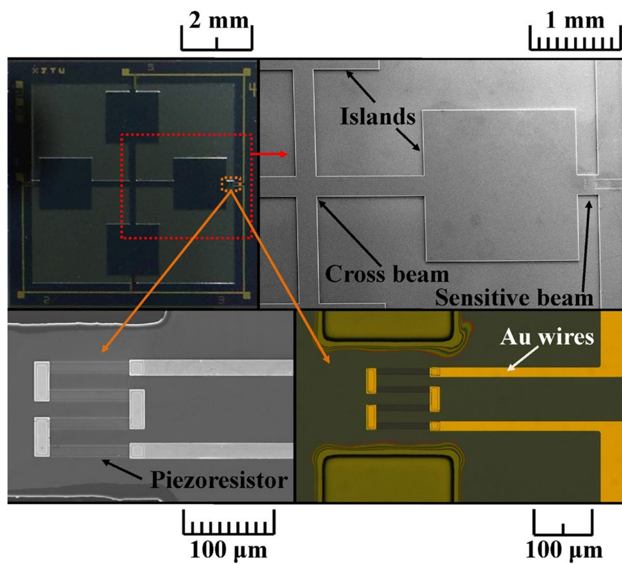

Fig. 6 The SEM and CCD photos of the fabricated BMQI sensor die

For the connections of resistors and formations of bonding pads, metallization process is performed to sputter Au. Furthermore, ohmic contacts between Au wires and piezoresistors are reinforced by sintering process. With the purpose of creating a cavity, forming islands and reducing the heights of islands, KOH etching is used on the back side of the wafer after patterned.

Afterwards, as an absolute pressure sensor is expected, the back side of the wafer is attached to Pyrex 7740 glass under vacuum condition, with anti-adsorption electrodes made of Cr sputtered on the glass by anodic bonding process. Finally, inductively coupled plasma (ICP) etch is involved to form beams on the front side.

The fabricated BMQI sensor die is shown in Fig. 6, where SEM images and CCD photograph are displayed as partial enlarged views.

4 Measurements and results

The package for measurements is built up as shown in Fig. 7. Figure 7a shows the sintering tube, header plate, gold-filled copper pins, sensor die and gold wires successively.

The sensor die is adhered to the header plate of the sintering tube by silica gel, which acts as a thermal stress isolation member to reduce error generated by thermal mismatch between the glass base of sensor die and the header plate. The rubber ring, shown in Fig. 7b, is used to seal the interstice between the inner sintering tube and the outer tube to isolate the sensor die from ambient environment, so as to create a hermetic cavity for absolute measurements. Each pad of the sensor die is electrically coupled to an associated columnar pin by a gold feedthrough to output the signal as shown in Fig. 7c. Figure 7d shows the package for measurements.

To describe the static characterization, a complete experimental setup is established in Fig. 8. The compressor acts as a pressure source. The sensors are calibrated with a reference pressure monitor (FLUKE A100K), excited by a 3 V DC power supply (RIGOL DP1116A), and outputs are measured by a multi-meter (KEITHLEY 2000).

Calibration results are plotted in Fig. 9, where the output voltage as a function of pressure is presented. The pressure is varying from 20 to 500 Pa at room temperature. In the figure, the calibrated data of five-round journey are described with solid line fixed by least square fitting and error bars. Meanwhile the simulation results of the designed model represented by double dot dash lines are employed to compare with the testing data. To gain an obvious comparison, the double dot dash lines have been moved to make the zero points of these two lines coincident. The sensitivity together with other static characteristics is calculated on the basis of least square fitting results, and listed in Table 1.

To assess the dynamic performance approximately, another BMQI sensor die from the same silicon wafer but with a through-hole on the glass base is utilized. The hole makes the pressures inside and outside the cavity equal, thus the applied atmosphere is equivalent to zero, and the sensor chip is only affected by vibration acceleration, which is convenient for dynamic experiments. A stable centrifugal machine is used for acceleration calibration

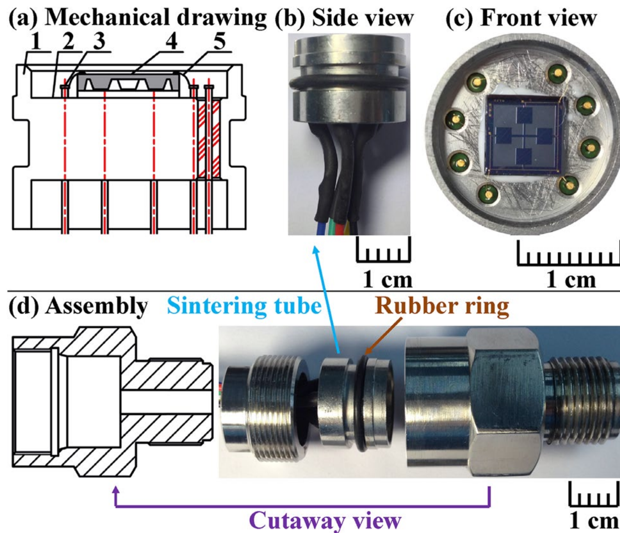

Fig. 7 The package of BMQI sensor die for measurements

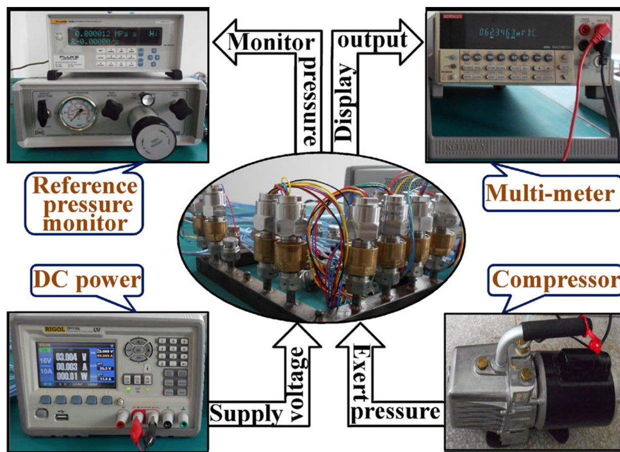

Fig. 8 Schematic diagram of the static calibration system

along the z-axis of BMQI. Through changing the rational speed, accelerations up to 15 g with an interval of 2.5 g are imposed. Figure 10 shows the experimental results of five-round journey, and the double dot dash line represents the simulation results of the designed model. According to the results, the maximum interfering signal is 1.274 mV/15 g. Besides, the standard errors of testing points that are partially presented by error bars in Figs. 9 and 10, are listed in Table 2. The natural frequency is evaluated through testing the BMQI with a hole. By fixing both the tested BMQI and a reference sensor on a shaker, a peak concerning the voltage ratio of these two sensors will be generated when a sine sweep frequency passes through. The peak induced by the structure resonance is plotted in Fig. 11, that reflects a resonant frequency of 10.275 kHz. Although slightly different damping factors and minor fabrication variations are

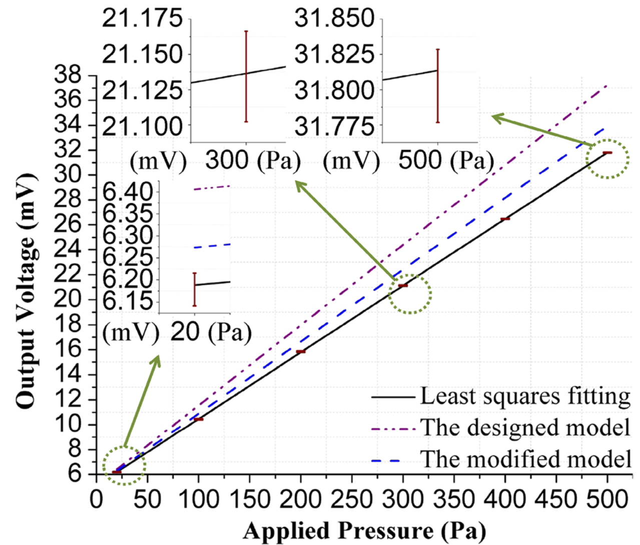

Fig. 9 Experiment and simulation results of the output voltage versus applied pressure

Table 1 The performances of the BMQI sensor

Parameter	Value
Reference temperature (°C)	20
Supply voltage (V)	3
Output under atmosphere (mV)	1,413.3
Zero point offset (mV)	5.121
Temperature coefficient of offset (/°C)	−0.00428
Full scale span (mV)	26.693
Sensitivity (μV/V/Pa)	17.795
Nonlinearity (%FS)	0.1405
Hysteresis (%FS)	0.2847
Repeatability (%FS)	1.4788
Accuracy (%FS)	1.5125

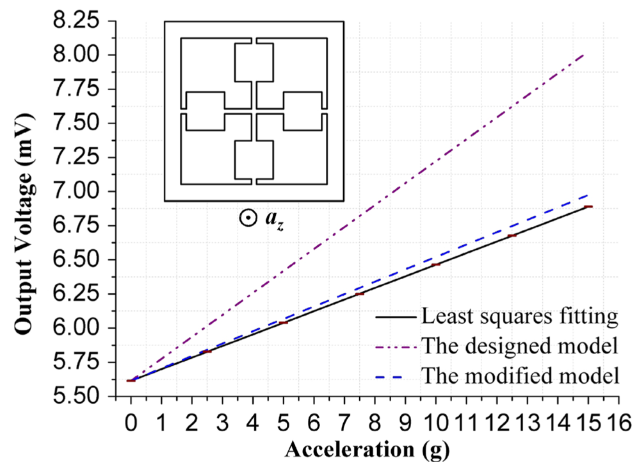

Fig. 10 Experiment and simulation results of the output voltage versus applied acceleration

Table 2 The standard errors of testing points in experiments

Testing point number	Corresponding pressure (Pa)	Standard error	Corresponding acceleration (g)	Standard error
1	20	0.03707	0	0.00145
2	100	0.03516	2.5	0.00159
3	200	0.06180	5	0.00174
4	300	0.03205	7.5	0.00152
5	400	0.02958	10	0.00177
6	500	0.02592	12.5	0.00194
7	–	–	15	0.00196

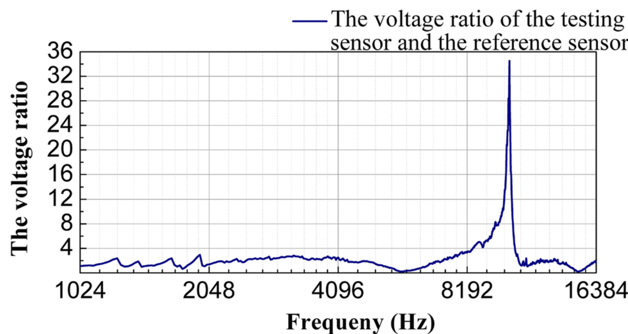

Fig. 11 The modal analysis result of the BMQI structure

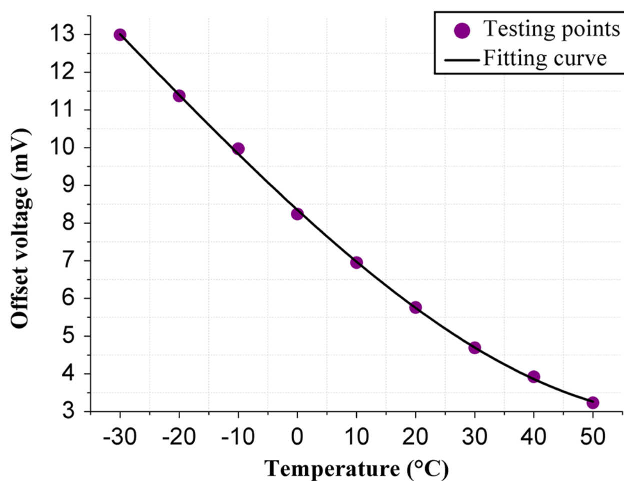

Fig. 12 The characteristic of the BMQI sensor's temperature drift

existent, the experiments are still significant for evaluating the dynamic performance of BMQI sensor under near-vacuum condition.

To describe thermal stability of the BMQI sensor, the temperature coefficient of offset (TCO) is measured within the range of −30 to 50 °C. Figure 12 shows the drift at the pressure of 12 Pa, which is the lowest pressure that the compressor can reach. In the figure, each point is recorded at intervals of an hour, and the measuring results are expressed by cubic polynomial fitting

$$U_o(T) = 5.42003 \times 10^{-9}T^3 - 3.87753 \times 10^{-6}T^2 + 7.61738 \times 10^{-4}T - 0.02088 \tag{10}$$

where U_o (T) is the output voltage at the temperature T. Based on the definition in the report by Jiachou and Xinxin (2010), the TCO at the temperature T can be deduced:

$$TCO(T) = \frac{U_o(T+\Delta T) - U_o(T)}{\Delta T \cdot U_{FS}(T)} = \frac{U'_o(T)}{U_{FS}(T)} \tag{11}$$

where U_o $(T + \Delta T)$ is the output voltage at the temperature $T + \Delta T$, ΔT the change in temperature, U_{FS} (T) the full scale output voltage at the temperature T, U'_o (T) the derivative of U_o (T). By combination of Eqs. (10) and (11), the TCO at the reference temperature is deduced and listed in Table 1. Additional specification is that the same power supply is used during all experiments.

5 Discussion

The BMQI sensor presents relatively better performances in sensitivity and overload resistance. In contrast with the beam-membrane sensor developed by Tian et al. (2012), the sensitivity is improved by 10.5 times. The sensitivity of the BMQI sensor is 48.292 % higher than the highest one of the sensors developed by Berns et al. (2006), and the overload resistance is more than 1.7 times higher. Additionally, as the bulk silicon micromachining technology has been utilized low cost and high yield have been achieved, unlike the report by Berns et al. (2006), in which SOI has been used to produce ultrathin film to acquire high sensitivity.

Obvious simulation errors about the designed model are existent in Figs. 9 and 10, due to the lack of sufficient space for convex corner compensation. To study the influences of convex corner undercutting, the model is modified based on the fabricated sensor die as shown in Fig. 13. In the figure, the corners are undercut and substituted by new ones at the places of slow corrosion rate. The variable U that reflects

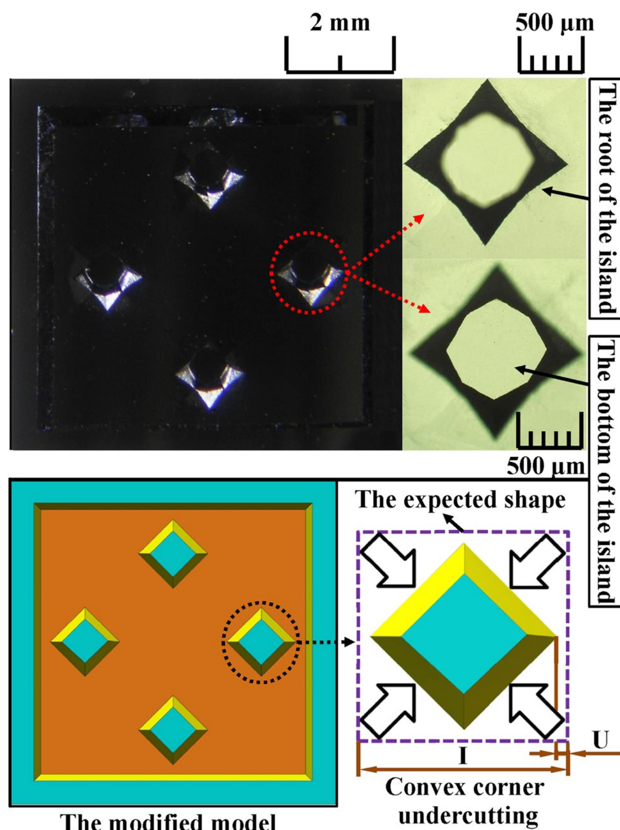

Fig. 13 Photos of undercut islands and schematic diagrams of the modified model

the distance between the new corners and the boundary of expected shape is determined to approximately 60 µm according to actual measurements. Simulation results of the modified model are also plotted in Figs. 9 and 10. The modified model presents obviously decreased simulation errors of 7.957 % FS, 6.658 % FS and 2.336 % corresponding to pressure, acceleration and modal analyses. In general, compared with the designed model, the convex corner undercutting decrease the dynamic interfering by 89.253 % FS. The natural frequency is enhanced by 22.356 % at the sacrifice of 20.326 % FS sensitivity, that is worth for improving the comprehensive performance.

Signal decoupling is critical for improving the accuracy of pressure measurements under dynamic condition. Since the applied pressure p and z-axis acceleration a_z are linearly related to the output voltage U_o, as described in the Eqs. (8) and (9), these two equations can be superposed to express the coupled signal U_o (p,a_z). As long as the small deflection theory is still applicable. The superposed equation based on the modified model is obtained as follows:

$$U_o(p, a_z) = 5.76330 \times 10^{-5} p + 9.24234 \times 10^{-6} a_z \quad (12)$$

where a maximum deviation of 0.01129 % from ANSYS® simulation results is verified. Thus the Eq. (12) can almost describe the coupled signal under the vibration environment. To decouple the signal, the BMQI sensor chip with a through-hole on the glass is required. As it is unaffected by pressures, the applied pressure can be set to zero. Therefore this senor chip is only affected by the term of acceleration in Eq. (12). Regardless of the fractionally different damping factors and tiny processing errors, the differential readout of these two BMQI sensor chips can extract the pressure term in Eq. (12) and achieve the decoupling.

6 Conclusions

This work attempts to introduce sensitive beams and multi islands into flat diaphragm to improve sensitivity and overload resistance of existing sensors. The scheme provides a solution to enhance sensitivity and overload resistance simultaneously. Experimental results have demonstrated the feasibility of the scheme. Future work will be devoted to designing the circuit for dynamic decoupling. The differential readout of the two BMQI sensor chips under acceleration will be experimentally measured to verify the decoupling scheme discussed.

Acknowledgments This work is supported by the National Science Foundation for Distinguished Young Scholars of China (No. 51325503), Young Scientists Fund of the National Natural Science Foundation of China (No. 51305336), National High Technology Research and Development Program of China (863 Program) (No. 2013AA041108), the Program for Changjiang Scholars and Innovative Research Team in University of China (No. IRT1033), and Postdoctoral Science Foundation of China (No. 2013M532036).

References

Bao MH, Yu LZ, Wang Y (1990) Micromachined beam-diaphragm structure improves performances of pressure transducer. Sens Actuators A Phys 21(1–3):137–141

Barlian AA, Park W-T, Mallon JR Jr, Rastegar AJ, Pruitt BL (2009) Review: semiconductor piezoresistance for microsystems. Proc IEEE 97(3):513–552. doi:10.1109/jproc.2009.2013612

Berns A, Buder U, Obermeier E, Wolter A, Leder A (2006) AeroMEMS sensor array for high-resolution wall pressure measurements. Sens Actuators A Phys 132(1):104–111. doi:10.1016/j.sna.2006.04.056

Chang L (ed) (2008) Foundations of MEMS, 1st edn. China Machine Press, Beijing

Clark SK, Wise KD (1979) Pressure sensitivity in anisotropically etched thin diaphragm pressure sensors. IEEE Trans Electron Devices 26(12):1887–1896

Eaton WP, Smith JH (1997) Micromachined pressure sensors: review and recent developments. Smart Mater Struct 6(5):530–539. doi:10.1088/0964-1726/6/5/004

Guiming Z, Libo Z, Zhuangde J, Shuming Y, Yulong Z, Enze H, Rahman H, Xiaopo W, Zhigang L (2011) Surface stress-induced deflection of a microcantilever with various widths and overall microcantilever sensitivity enhancement via geometry modification. J Phys D Appl Phys 44(42):425402. doi:10.1088/0022-3727/44/42/425402

Hopcroft MA, Nix WD, Kenny TW (2010) What is the Young's modulus of silicon? J Microelectromech Syst 19(2):229–238. doi:10.1109/jmems.2009.2039697

Jiachou W, Xinxin L (2010) A high-performance dual-cantilever high-shock accelerometer single-sided micromachined in (111) silicon wafers. J Microelectromech Syst 19(6):1515–1520. doi:10.1109/jmems.2010.2076783

Johnson RH, Karbassi S, Sridhar U, Speldrich B (1992) A high-sensitivity ribbed and bossed pressure transducer. Sens Actuators A Phys 35(2):93–99. doi:10.1016/0924-4247(92)80146-t

Ko HS, Liu CW, Gau C (2007) Micropressure sensor fabrication without problem of stiction for a wider range of measurement. Sens Actuators A Phys 138(1):261–267. doi:10.1016/j.sna.2007.04.065

Lin L, Chu H-C, Lu Y-W (1999) A simulation program for the sensitivity and linearity of piezoresistive pressure sensors. J Microelectromech Syst 8(4):514–522

Mackowiak P, Schiffer M, Xin X, Obermeier E, Ha-Duong N (2010) Design and simulation of ultra high sensitive piezoresistive MEMS sensor with structured membrane for low pressure applications. In: 2010 12th Electronics Packaging Technology Conference (EPTC 2010), pp 757–761. doi:10.1109/eptc.2010.5702738

Quan W, Jianning D, Wenxiang W (2005) Fabrication and temperature coefficient compensation technology of low cost high temperature pressure sensor. Sens Actuators A Phys 120(2):468–473. doi:10.1016/j.sna.2005.01.036

Reynolds JK, Catling D, Blue RC, Maluf NI, Kenny T (2000) Packaging a piezoresistive pressure sensor to measure low absolute pressures over a wide sub-zero temperature range. Sens Actuators A Phys 83(1–3):142–149. doi:10.1016/s0924-4247(00)00294-6

Shimazoe M, Matsuoka Y, Yasukawa A, Tanabe M (1982) A special silicon diaphragm pressure sensor with high output and high-accuracy. Sens Actuators 2(3):275–282. doi:10.1016/0250-6874(81)80047-9

Sze SM (ed) (1994) Semiconductor sensors, 1st edn. Wiley, New York

Tian B, Yulong Z, Zhuangde J, Bin H (2012) The design and analysis of beam-membrane structure sensors for micro-pressure measurement. Rev Sci Instrum 83(4):045003. doi:10.1063/1.3702809

Timoshenko S, woinosky-Krieger S (eds) (1987) Theory of plates and shells. 2nd edn. McGraw Hill Classic Textbook, New York

Tufte ON, Stelzer EL (1963) Piezoresistive properties of silicon diffused layers. J Appl Phys 34(2):313–318. doi:10.1063/1.1702605

Young WC (ed) (1986) Roark's formulas for stress and strain, 6th edn. McGraw-Hill, New York